Nanotechnology enabled design of a structural material with extreme strength as well as thermal and electrical properties

M. Rajagopalan [1], K.A. Darling [2], C. Kale [1], S.A. Turnage [1], R.K. Koju [3], B.C. Hornbuckle [2], Y. Mishin [3], K.N. Solanki [1],*

[1] School for Engineering of Matter, Transport, and Energy, Arizona State University, Tempe, AZ 85287, USA
[2] Army Research Laboratory, Weapons and Materials Research Directorate, APG, MD 21014, USA
[3] Department of Physics and Astronomy, George Mason University, MSN 3F3, Fairfax, VA 22030, USA

The potential benefits of nanocrystalline (NC) alloys for use in various structural applications stem from their enhanced mechanical strengths. However, deformation-induced grain growth in NC materials reduces the strength and is a widely reported phenomenon occurring even at low-temperatures. Controlling such behavior is critical for the maturation of bulk nanocrystalline metals in various advanced engineering applications. Here, we disclose the mechanism by which grain boundary sliding and rotation are suppressed when a NC material is truly thermo-mechanically stabilized against grain growth. Unlike in any other known nanocrystalline metals, the absence of sliding and rotation during loading, at extreme temperatures, is related to short-circuit solute diffusion along the grain boundaries causing the formation of solute clusters and thus a significant change of the grain boundary structures. The departure of this unusual behavior from the well-established norm leads to a strong enhancement of many mutually exclusive properties, such as thermo-mechanical strength, creep resistance, and exceptionally high electrical/thermal conductivity. This work demonstrates that Cu-based nanocrystalline alloys can be used in applications where conventional Cu-based polycrystalline materials are not viable.

Introduction

The potential benefits of nanocrystalline (NC) alloys, i.e., materials with a mean grain size (*d*) below 100 nm, for use in various structural applications stem from their enhanced mechanical strengths resulting from a reduced grain size. However, these NC materials often exhibit poor microstructural stability and grain growth under combined thermal (low or high temperatures) and mechanical loads compared to their coarse grained counterparts (e.g., [1–4]). Controlling the grain growth is critical for advanced structural applications such as next generation heat exchangers, high-end electronics, high-speed rail contact wires, and high-speed pulse magnets. For such applications, the quest has been to develop and design new alloys that exhibit a combination of extremely high strength, low strain rate sensitivity (high creep resistance), and/or high electrical/thermal conductivity. Materials required for such applications are expected to maintain a multitude of mutually exclusive properties when exposed to high pressures and temperatures for tens of thousands of hours. For instance, for a high-speed pulse magnets, annealed copper (IACS) generally exhibits a low electric resistivity of 1.72×10^{-8} Ω·m (100% IACS). However, the strength and thermal stability of the annealed copper and related alloys is relatively low for structurally demanding applications [5]. Similarly, for the heat exchanger applications, generally the high temperature strength of metal-based alloys is extremely low, i.e., on the order of 30–50 MPa at 800 °C for the best Ni-based heat exchanger currently in use [6]. In effort to produce copper with

---

* Corresponding author.
E-mail address: Solanki, K.N. (kiran.solanki@asu.edu).

1369-7021/ https://doi.org/10.1016/j.mattod.2019.09.024

extremely high strength and good electrical/thermal conductivity, various fine-scale two-phase composite materials [5,7,8], such as Cu-Nb microcomposites [9], and second-phase strengthened Cu-Ag alloys [10,11] have been developed. For instance, the Cu-Nb [12], Cu-Ag [13] and Cu-Cr [14] alloys exhibit the room temperature yield/ultimate strength of about 700–1200 MPa, 794–890 MPa, and 430–840 MPa along with the electrical resistivity of 85–55% IACS, 76–72% IACS, and 75–85% IACS, respectively. However, the poor thermal stability of the structure and the strain rate sensitivity (SRS) of these alloys are limiting their practical applications. Apart from the microstructural stability, in general, most nanocrystalline/ultrafine grained materials tend to have either high strength and low electrical conductivity or low strength and high electrical conductivity [5]. A critical review of the strength and electrical conductivity of structural alloys with various average grain sizes can be found in [5] and references within.

On the other hand, in NC face-centered-cubic (FCC) metals, such as pure copper with its average yield strength of 610 MPa and resistivity of 95% IACS, the strain rate sensitivity (SRS) factor m increases significantly even at ambient conditions [15]. For instance, room temperature m values for coarse-grained (CG) polycrystalline, ultra-fine grained (UFG), and NC Cu under compression are 0.009 ± 0.002, 0.020 ± 0.007, and 0.038 ± 0.006, respectively [16]. For grain sizes of about 10 nm, m values as high as 0.06 have been reported [17]. Such enhanced m values in NC FCC metals are due to the increase in the grain boundary volume fraction as compared to the conventional, CG materials. In addition, it is well known that NC Cu and other single-component metals are extremely sensitive to grain growth, rapidly coarsening to micrometer-scale grains during loading and deformation at low and moderate temperatures. As a result, such materials are not viable for applications requiring a combination of high mechanical strength, creep resistance, and high electrical/thermal conductivity. Contrary to this common belief, we provide here extensive evidences that in truly stabilized NC materials, the thermo-mechanical strength, the SRS, and conductivity, which are mutually exclusive properties in nature, can coexist in such materials and be tailored for advanced applications.

The NC Cu-Ta alloy presented here can be produced in quantities far exceeding the laboratory scale. Kilogram quantities of the alloys have been manufactured into sizeable, fully dense bulk parts, see Fig. A1. The material exhibits the yield strength of over 1 GPa and a 71% IACS electrical conductivity along with a lowest reported SRS at 80% of the melting point (refer to Fig. A2 for the melting temperature of the material). The key physical mechanisms behind this remarkable phenomenon are related to the kinetic pinning behavior, which results in full stabilization of the nano-grains. Further, the NC Cu-Ta alloy retains significant portion of the coarse-grained pure Cu electrical and thermal conductivities. Overall, these findings demonstrate and clarify that the microstructural stability controls extreme SRS, strength and conductivity, and thus has the potential to be used in advanced engineering applications.

Results and discussion

Unique thermo-mechanical responses and anomalous strain rate sensitivity behavior

The NC Cu-10 at.% Ta alloy (referred to herein as NC Cu-Ta) studied in this work is a model material system to provide evidence that the microstructural stability controls extreme SRS, resulting in high strength, creep resistance and high electrical/

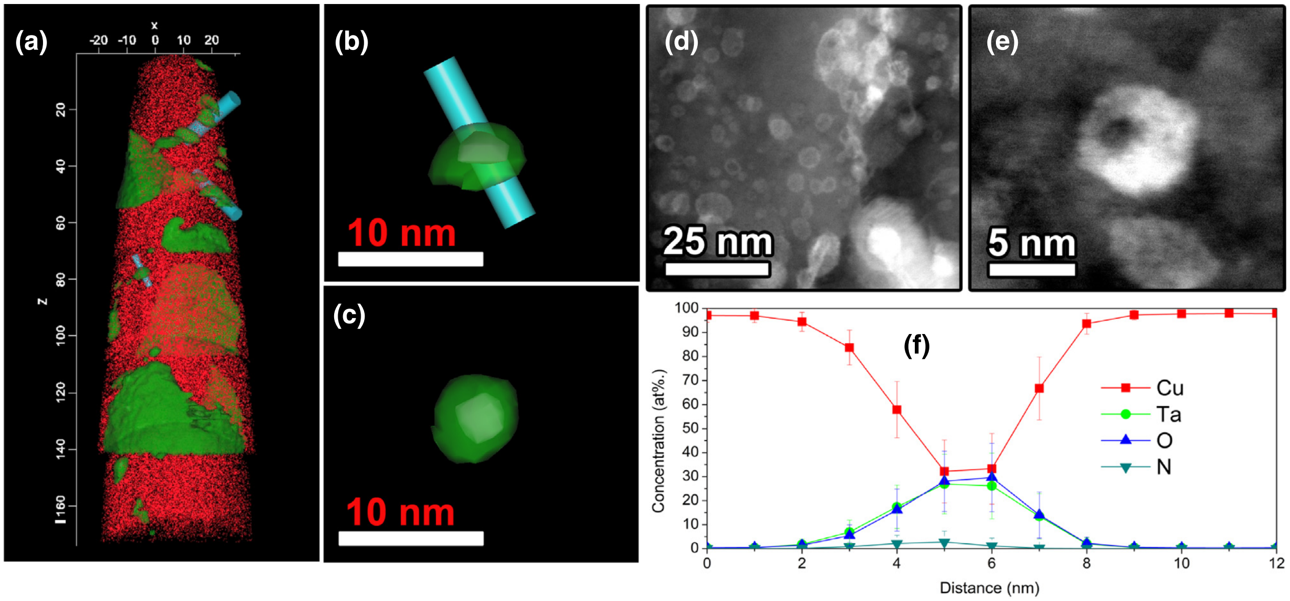

FIGURE 1

(a) Atom map of Cu in NC Cu-Ta using 6 at.% Ta isoconcentration surfaces (green), showing multiple probing cylinders passing through Ta particles. (b) A cylinder passing through a selected 6 at.% Ta isoconcetration surface surrounding a 21% O isoconcentration surface, indicating a core–shell structure for the Ta particle. (c) A top down view of Figure (b) showing the O surface roughly centered with respect to x and y dimensions within the Ta surface. (d) HAADF-STEM image accentuating tantalum-rich clusters on the basis of atomic-number contrast. e) High-magnification HAADF image a Ta nanocluster. (f) 1D concentration profile generated from the cylinder shown in Figure (b), showing a representative chemical composition for the core–shell Ta particles.

thermal conductivity. The material was produced by high energy ball milling followed by equal channel angular extrusion [18,19] (See Methods). This alloy was previously studied by limited mechanical testing, such as high temperature creep measurements [18,19]. Primary microstructural characterization using transmission electron microscopy (TEM) revealed the presence of copper grains with an average size of 50 ± 18 nm as well as tantalum particles. The latter exhibited a range of sizes from atomic-scale particles ($d < 14$ nm) to larger particles ($d > 14$ nm). Their average diameters were found to be 3.18 ± 0.9 nm and 32 ± 8 nm, respectively. These size distributions were obtained from areas similar to that seen in the Extended Data Fig. 2 of [19], which was averaged over 300 grains. It is important to note that the microstructure has a few twins, but the formation of nanotwins during the processing for this chemical composition was minimal due to the presence of the fine nanoclusters [20]. Further, the smaller Ta clusters (average diameter of 3.18 ± 0.9 nm) have a complex structure/chemistry as shown in Fig. 1. Here, the atom probe analysis captures the size and distribution of Ta (green) particles/clusters using a 6 at.% Ta isoconcentration surfaces within the Cu (red) matrix, Fig. 1(a). This size is comparable to that noted in the TEM images. The TEM images show that a large percentage of the Ta particles have a darker core structure when viewing in High Angle Annular Dark Field (HAADF) mode, which is indicative of a higher concentration of a low atomic number element present within the core relative to the outer shell (Fig. 1(d–e)). A combination of isoconcentration surfaces and 1D profiles, Fig. 1(b–d), confirms an enrichment in O within the core structure of such particles, while the outer shell is only composed of Ta and Cu. This analysis, along with previous work, indicates that the particles/clusters have a chemical distribution of both Ta and O ranging from 10 to 90 at.% for Ta and 2–50 at.% for O, with the remaining balance composed of Cu [21]. Additionally, O was generally found to be localized in the core of the Ta particles/clusters, while the O concentration in the Cu matrix is less than 1 at.%.

Conventional compression tests were performed over a wide range of applied deformation rates (10^{-4}–10^{1} s^{-1}) and temperatures (297–1273 K) (see Methods). Previous studies in CG polycrystalline and single-crystalline Cu [22–24] suggest that both tension and compression can be applied for measuring m. This is technologically important since many industrial operations, such as extrusion, rolling, forming, and forging to produce complex parts and geometries, create a variety of stress and strain rates in the material. Typical true stress–strain curves shown in Fig. 2a reveal several significant features. First, the absence of appreciable strain hardening (i.e., elastic-perfectly plastic behavior) at different deformation rates and temperatures suggests the absence of significant changes in grain size, morphology or texture during the deformation. Secondly, while the SRS is negligible at room temperature, the rate effect becomes more apparent as temperature is increased.

The SRS parameter m was computed from the relation $m = \partial \log(\sigma)/\partial \log(\dot{\varepsilon})$, where σ is the stress and $\dot{\varepsilon}$ the strain rate. Fig. 2b shows m as a function of strain and temperature. The SRS parameter is inversely proportional to the apparent activation volume v^*. The latter is critical in determining the rate-controlling mechanism of plastic deformation and is a measure of the average volume of the material involved in the deformation process. Fig. 2b thus reflects the evolution of the rate-controlling mechanisms with strain and temperature in the NC Cu-Ta alloy. The m values increase especially at higher temperatures. The higher m at lower strain values, as indicated by the five-fold increase in the spread of the m values over the given strain range (0.2–12.5%). This points to the more pronounced role played by the thermally activated strain hardening processes in dictating the SRS behavior at early stages of deformation.

The property maps (Fig. 3) highlight the anomalous behavior of NC Cu-Ta when compared to almost every structural material currently in use. For instance, although the SRS parameter m increases with temperature for all strains by almost a factor of 10 for NC Cu-Ta, it does not break the threshold of 0.3 expected for materials whose deformation is dominated by grain boundary processes such as creep. In fact, an extensive survey of over 184 coarse-grained alloys based on Zn, Sn, Mg, Al, Cu, Fe, Ni and Ti has shown that all alloys with stable grain sizes ~10–400 times the grain size in the NC Cu-Ta alloy (i.e., 1–20 μm), exhibit deformation associated with grain boundary processes and thus m values between 0.3 and 0.8 at homologous temperatures between 50 and 80% T_m [25] (T_m being the melting point), see Fig. 2b. This value should approach $m \sim 1$ for smaller grain sizes near T_m. The anomalously small m values found in the NC Cu-Ta alloy go totally against this general trend. Further, the 0.2% strength decrease with homologous temperature occurs much earlier in

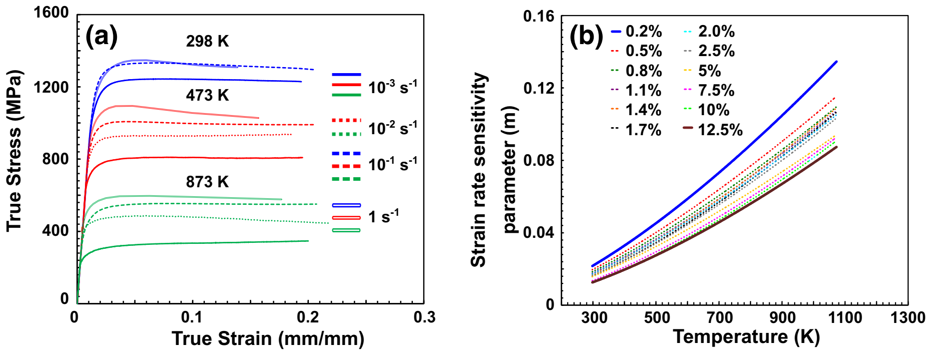

FIGURE 2

Stress–strain responses of NC Cu-Ta at different strain rates. (a) Low strain rate stress–strain response of NC Cu-Ta as a function of strain rate and temperature. (b) Effect of temperature on strain rate sensitivity of NC Cu-Ta at different strain levels measured from experiments.

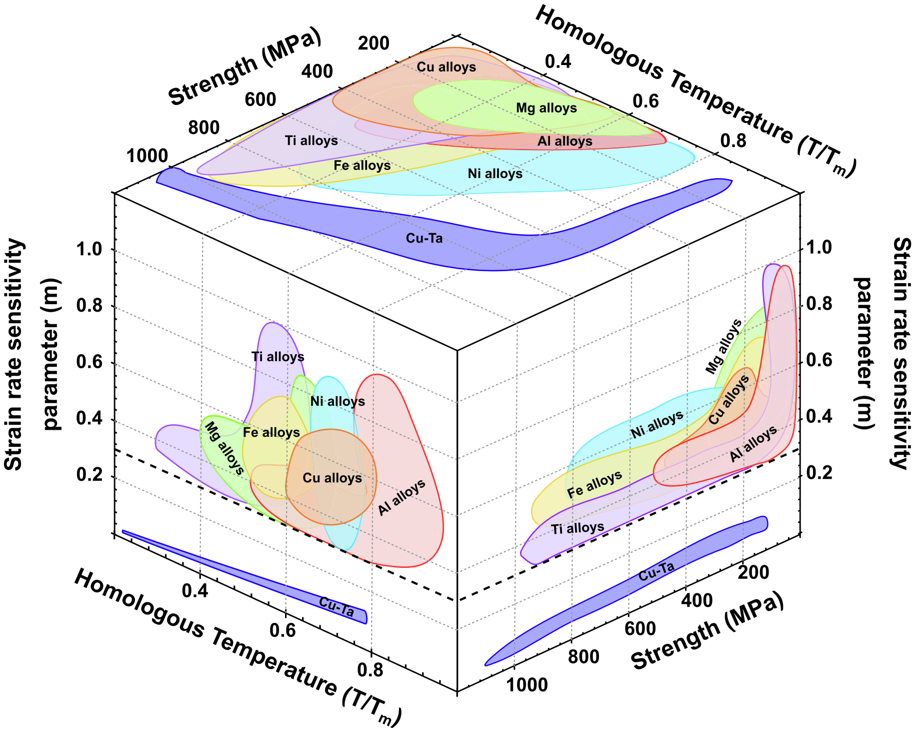

FIGURE 3

Material property maps, showing the strain rate sensitivity versus homologous temperature versus 0.2% strength of NC Cu-Ta in comparison with various coarse-grained structural alloys. The literature data are from Chapters 22 and 26 of [25].

conventional alloys than in NC Cu-Ta, which is a consequence of the remarkable thermo-mechanical stability of NC Cu-Ta.

Novel archetype microstructure of a NC alloy

Microstructural changes in NC Cu-Ta at elevated temperatures were examined by TEM. The Cu grain size and Ta nanocluster size distributions in Fig. 4a, b show very little change in either, despite being exposed to temperatures above the consolidation temperature of 973 K. The grain size increases from 50 ± 18 nm in the as-received to 89.7 ± 12.8 nm after mechanical testing at 1073 K (0.8 T_m). The Cu matrix grains are found to be equiaxed in shape and coexist with larger residual Ta particles, spheroidal in morphology, having an average diameter of 32 nm in both samples (Fig. 4c, d). Such small changes in microstructure are very surprising given that the average grain size is less than 100 nm. To evaluate the influence of the deformation rate and temperature on the textural changes, precession diffraction measurements were performed in various areas (Fig. 4e, f). The orientation imaging map (OIM) shows a high degree of randomness in the orientation relationships between the Cu grains in the as-received state as well as after the 1073 K testing with a texture index of one. Processes such as grain rotation and grain boundary sliding would lead to texturing as multiple grains reorient themselves to accommodate slip and extensive plastic deformation, as is the case in typical NC metals. This observation suggests that the stable structure of the NC Cu-Ta alloys exhibits very limited grain rotation and growth even at 0.8 T_m.

Higher magnification aberration corrected scanning TEM (STEM) was used to resolve the underlying microstructural features in more detail. Figs. 4c, d and 5a, b illustrate that the Ta nanoclusters are distributed homogeneously in the grain interiors and at grain boundaries and interact with the dislocations. The average size of the nanoclusters was found to be 3.18 ± 0.9 nm in diameter with an average inter-nanocluster spacing of 5.2 ± 1.74 nm (Ta nanocluster chemical composition is shown in Fig. 1). These numbers remain nearly constant with the application of stress and temperature, highlighting the alloys stability and resistance to coarsening (Figs. 4b and 5c). It is owing to the stability and high density of the coherent nanoclusters present in the microstructure that the Cu grains remain almost unchanged (Fig. 5a, b). These observations suggest that the nanoclusters pin the grain boundaries and block the grain boundary sliding and grain rotation processes. The pinning of the grain boundaries is then responsible for imparting the extraordinary strength and structural stability to these alloys, and the breakdown of the universally expected mechanical behavior of NC materials. Further, the average value of m for the NC Cu-Ta alloy at 873 K is 0.089, which corresponds to an apparent activation volume of v^* $\sim 131b^3$, b being the magnitude of the dislocation Burgers vector. The activation volume v^* is obtained using the relation $v^* = \sqrt{3}kT/m\sigma$, where k is Boltzmann's constant, T is temperature in K, m is the SRS parameter and σ is the flow stress. This large activation volume is highly unusual for a NC material especially at these temperatures. Normally, deformation of NC materials is controlled by grain boundary processes such as sliding, grain rotation, and diffusional creep, for which v^* is relatively small, typically $\sim 1b^3$ [25]. For comparison, CG FCC metals generally have very large room temperature v^* values (100–1000s of b^3) since the deformation is associated with dislocation motion through a forest of dislocations, while grain boundary processes

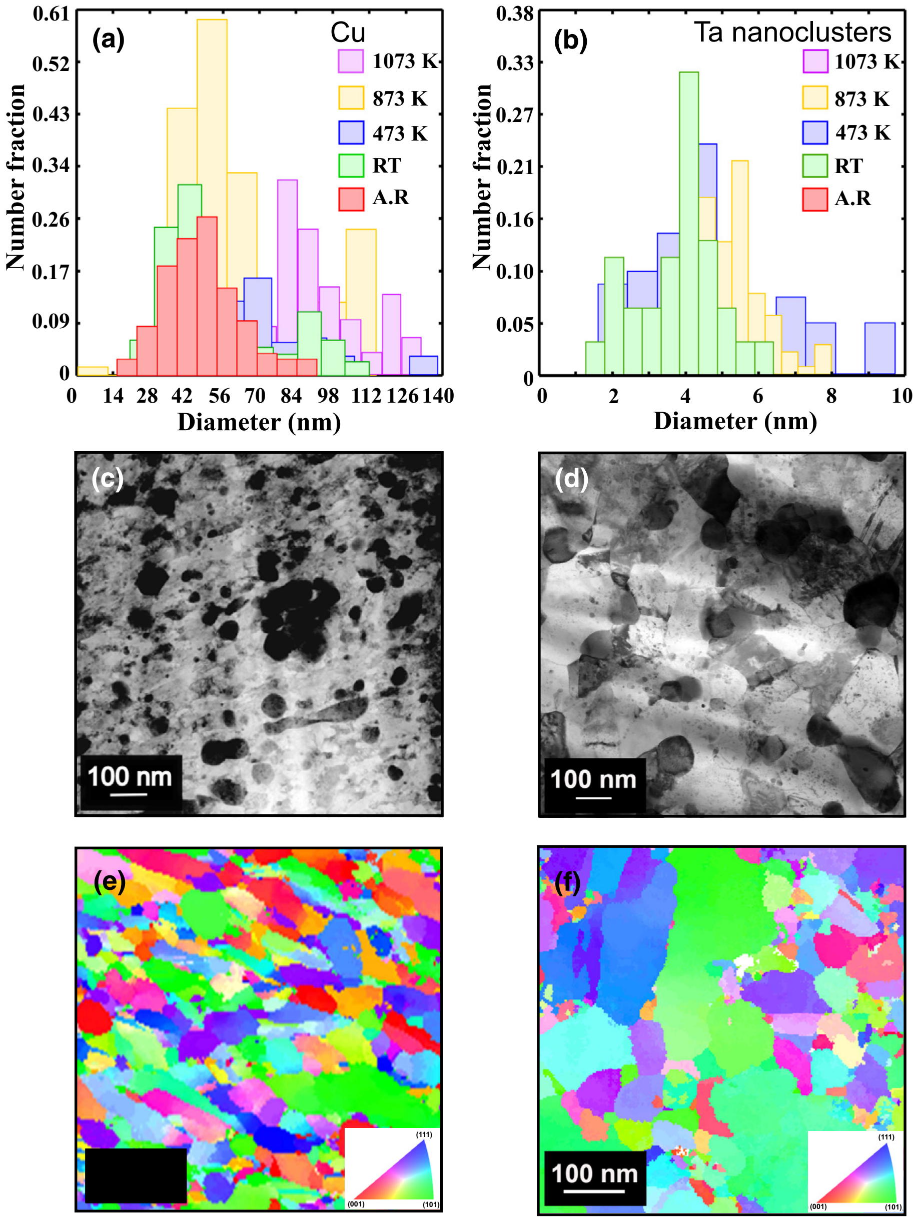

FIGURE 4

Size distribution of Cu grains and Ta nanoclusters in as-received (AR) and quasi-statically tested samples at the strain rate of 0.01 s^{-1}. (a) The distributions indicate nominal increase in Cu grain size with the majority of the grains remaining in the NC regime. (b) Ta nanoclusters also exhibit stability with temperature. (c) Bright field (BF) image of as-received sample. (d) BF image of quasi statically tested sample at 1073 K. (e) Precession diffraction image of as-received sample. (f) Precession diffraction image of quasi-statically tested sample at 1073 K.

play a secondary role. The values of v^* obtained for NC Cu-Ta are strongly shifted towards the latter scenario, confirming that the grain boundary mechanisms of deformation are effectively suppressed, see Fig. 5d.

Atomistic simulations of deformation behavior

To gain a deeper understanding of the fundamental mechanisms behind the extraordinary structural stability and strength of the NC Cu-Ta alloys, atomistic computer simulations were conducted employing molecular dynamics (MD) and Monte Carlo methods (see Methods). Four atomic percent of Ta was introduced into a Cu nanocrystal with an average grain size of 12.5 nm. This composition corresponds to the experimental Ta concentration in the NC Cu-Ta alloy outside the residual Ta grains. The sample was brought to thermodynamic equilibrium by semi-grand canonical Monte Carlo simulations. The Ta atoms were found to form nanometer-scale particles distributed at the grain boundaries and partially inside the grains. The sample was then subject to a series of uniaxial compression tests at the temperatures of 300 and 1000 K with different strain rates ranging from 10^6 to 10^9 s^{-1}. In agreement with the experiment, the stress–strain curves did not show any strain hardening. The flow stress σ (defined as the stress at 10% compression) was found to decrease with temperature and slightly increase with the strain rate (Fig. 6a), again in agreement with the experiments.

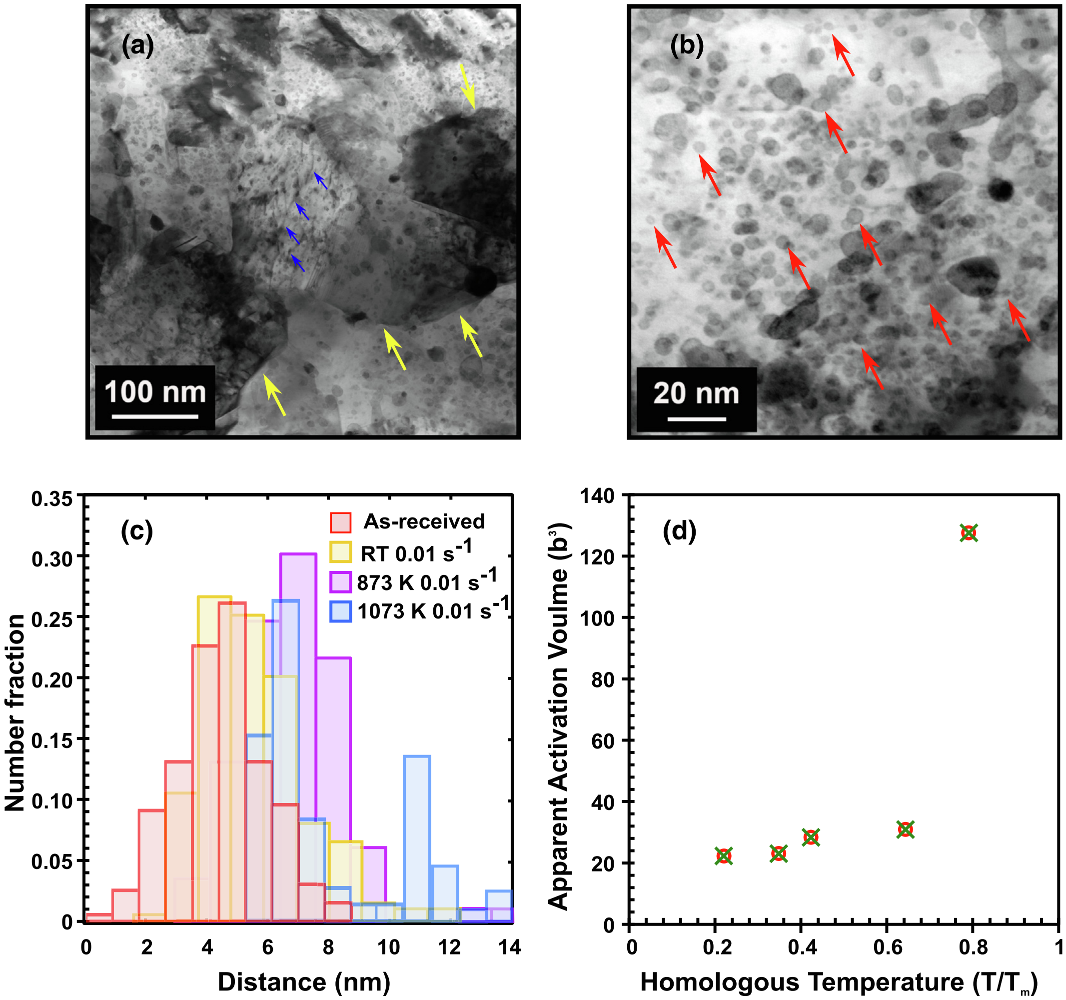

FIGURE 5

BF images of a sample tested quasi-statically (0.01 s^{-1} strain rate) at 1073 K showing Ta nanoclusters along with the average inter-nanocluster spacing distribution. (a) BF image. (b) Higher magnification BF image showing distribution of Ta nanoclusters. (c) Inter-nanocluster spacing distribution in as-received and quasi-statically tested samples at room temperature, 873 K and 1073 K. (d) Apparent activation volume (b^3) in NC Cu-Ta plotted as a function of homologous temperature. Blue arrows in Figure (a) indicate dislocations and the yellow arrows indicate Cu grain boundaries. The small Ta nanoclusters are indicated by red arrows in (b).

The slopes of the curves in Fig. 6a show that the SRS increases with temperature, which was also found in the experiments (cf. Fig. 2b). For quantitative comparison, the SRS parameter m was computed from the simulation results. The values obtained were $m = 0.029 \pm 0.004$ at 300 K and $m = 0.075 \pm 0.004$ at 1000 K. These numbers agree reasonably well with the experimental numbers (Fig. 2b). Examination of microstructures before and after the deformation did not reveal any changes in the grain size or Ta nanocluster distribution, confirming the high structural stability. By contrast, similar deformation tests performed on NC Cu (same initial grain size) resulted in significant grain growth and larger SRS. Furthermore, Fig. 6b, c demonstrate that the grain boundary sliding and grain rotation processes occurring during the deformation are much less pronounced in the NC Cu-Ta alloy than in NC Cu. Such processes constitute the basic mechanisms governing the deformation of nano-grains at high homologous temperatures. Their absence in NC Cu-Ta signals a reversal of the known deformation response that commonly occurs in other NC materials. Fig. 6d, e show that, as the Ta concentration increases, the grain area and the misorientation angles remains almost constant during the MD simulations. This suggests that the grain growth and the grain sliding/rotation processes are significantly reduced and eventually shut down as the Ta concentration is increased. It is important to note that the maximum size of the Ta nanoclusters is not the criterion for blocking grain boundary motion and sliding mechanisms. Instead, the important parameter is the number density of the Ta nanoclusters needed to exert the pinning force on the grain boundaries leading to microstructure stability [26]. This is consistent with the previous work, which has shown that the size of the Ta nanoclusters is independent of the Ta concentration, while only their number density depends on the Ta concentration [21,26].

To further demonstrate that the structural stability of the Cu-Ta alloy is caused by the pinning of grain boundaries by Ta nanoclusters, a different simulation setup was created in which a cylindrical grain with a circular cross-section was embedded in a larger grain serving as a matrix. In a recent study of this system

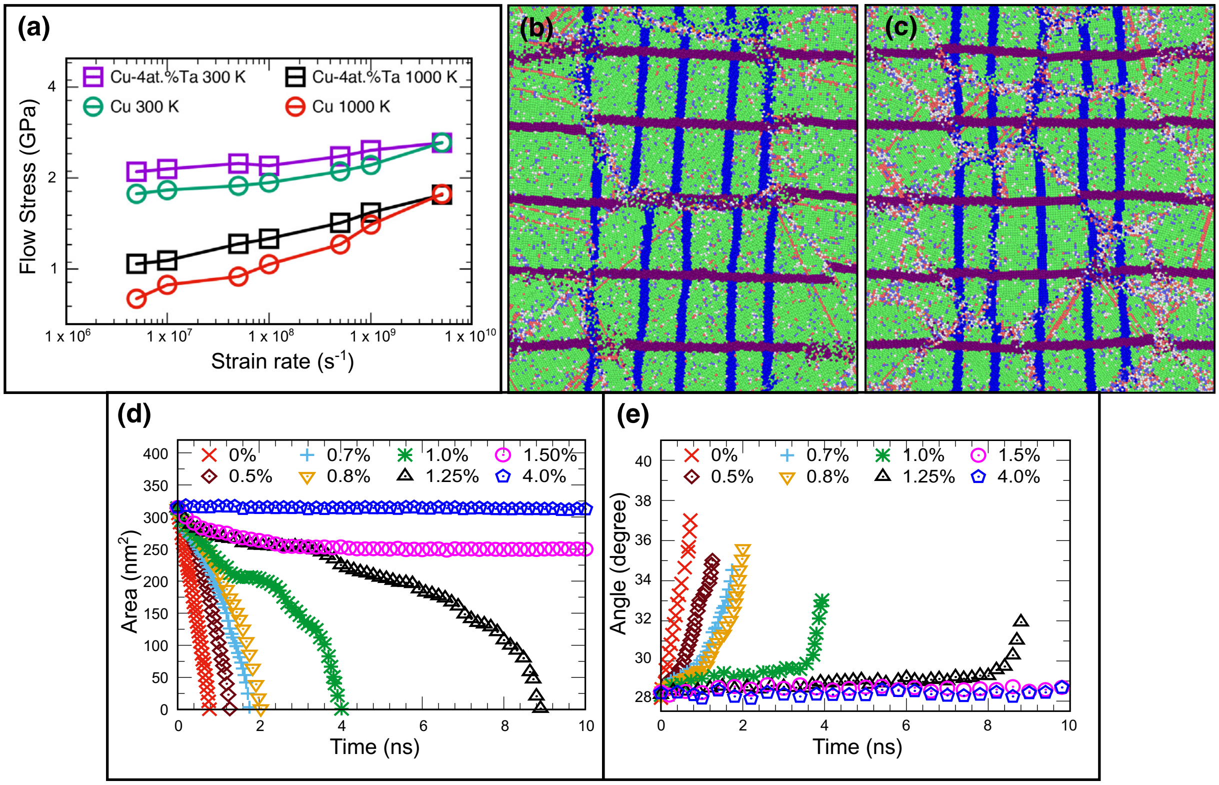

FIGURE 6

(a) Flow stress as a function of strain rate (s^{-1}) in NC Cu and NC Cu-4 at.%Ta alloy in MD simulations at 300 K and 1000 K. (b) Typical projection of NC Cu after 10% compression with the strain rate of $5x10^6$ s^{-1} at 1000 K. The compression direction is horizontal. The horizontal (purple) and vertical (blue) stripes represent two sets of artificial marker lines. (c) Same as (b) but for the NC Cu-4 at.%Ta alloy. The discontinuities and rotations of the marker lines are indicators of grain boundary sliding and grain rotation. Grain area (d) and misorientation angle (e) as functions of time in MD simulations of a cylindrical grain at 900 K. The alloy compositions (at.%Ta) are indicated in the label. The initial misorientation angle is 28°.

in pure Cu [27,28], such a grain was found to shrink under capillary forces and simultaneously rotate towards larger misorientation angles. In this work, Cu was replaced by a random Cu-Ta solid solution mimicking the metastable state of the alloy after mechanical alloying. In alloys with small Ta concentration, the grain was found to shrink and rotate, although slower than in pure Cu due to the solute drag effect. When the composition reached ~1.5 at.%Ta, the grain shrinkage and rotation practically stopped. In the alloy with 4 at.%Ta, the grain boundary did not move at all and the short-circuit Ta diffusion along the grain boundary resulted in the formation of a set of Ta nanoclusters that pinned the boundary in place. We can thus conclude that in the NC Cu-4 at.%Ta alloy, any grain boundary motion or grain rotation must be totally arrested by the Ta nanoclusters, which was indeed observed in the experiments. Since grain boundary sliding is a process coupled to grain boundary motion and grain rotation [29,30], this process is blocked as well. In addition to suppressing the SRS, these findings also explains in part the mechanisms responsible for the extraordinary creep resistance reported for this alloy [19].

Finally, the electrical conductivity (σ) of the NC-Cu-Ta was probed at room temperature using a Meandering Winding Magnetometer (MWM). The thermal conductivity (κ) was estimated from the electrical conductivity by applying the Wiedemann-Franz Law of $\kappa/\sigma = LT$, where L is the Lorentz number and T is temperature. The results are plotted in Fig. 7 in comparison with pure Cu and various Cu-based alloys. Fig. 7a indicates that for NC Cu-Ta, the strength is significantly improved while maintaining a relatively high electrical conductivity, i.e., yield strength of over 1 GPa along with an 71% IACS electrical/thermal conductivity. Typically, as the grain size decreases, the electric resistivity increases due to the interface scattering of the carriers (Matthiessen's rule) that leads to decrease in the electrical conductivity of NC Cu-Ta as compared to pure coarse-grained Cu. However, the NC-Cu-Ta retains a significantly portion of the pure coarse-grained Cu electrical conductivity while reaching a high strength. To further address this trend, if we assume that the probability of reflection at the interfaces (Cu-Ta and grain boundary) is about $R = 0.25$, and the bulk Cu crystal mean free path of $\lambda = 40$ nm [32], then using the Mayadas and Shatzkes formula [33]

$$\frac{\sigma_{CuTa}}{\sigma_{Cu}} = 1 - \frac{3}{2}\beta + 3\beta^2 - 3\beta^3 \ln\left(1 + \frac{1}{\beta}\right) \tag{1}$$

where $\beta = \frac{\lambda}{d}\left(\frac{R}{1-R}\right)$, the approximate conductivity of NC Cu-Ta (σ_{CuTa}) is predicted to be about 71% that of a single-crystalline or CG Cu (σ_{Cu}), which is similar to the measured decrease in the electrical conductivity, as plotted in Fig. 7a. This may indicate

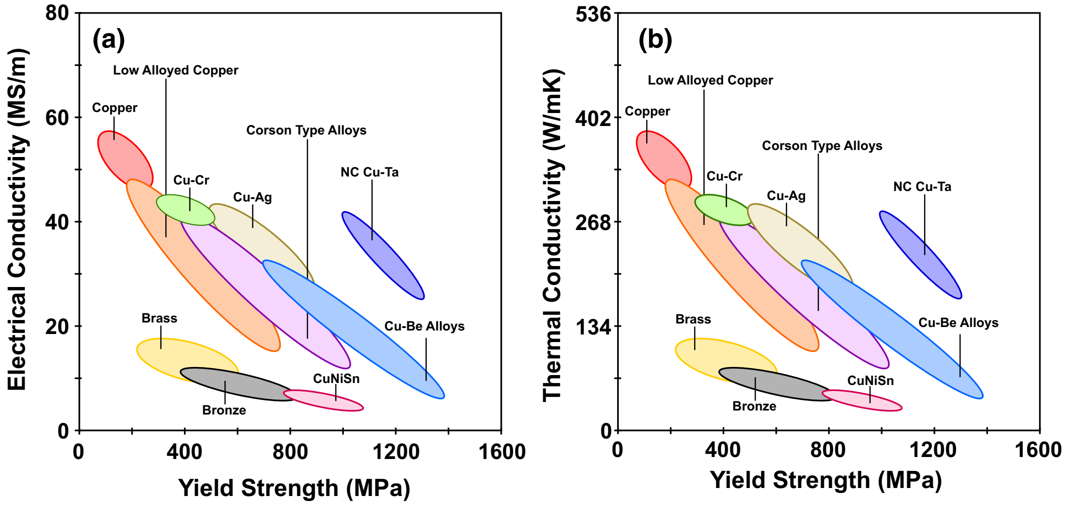

FIGURE 7

(a) Electrical and (b) thermal conductivities at room temperature versus 0.2% yield strength of pure Cu and various Cu based alloys. The variation in the NC Cu-Ta strength and conductivities are due to different Ta concentrations (1at%, 5at% and 10at% as well as changes in the average grain size). Overall, NC Cu-Ta exhibits yield strength of over 1 GPa along with an 71% IACS electrical conductivity. Note: literature electrical conductivity data where obtained from [31].

that the mean free path of conduction electrons in the NC Cu-Ta is governed by the average grain size, i.e., the nanoclusters are coherent-to-semi-coherent and their spacing (which is in the order of 5.2 ± 1.74 nm) does not control the electronic properties of NC Cu-Ta. Similar trends as observed with respect to the thermal conductivity. Fig. 7b shows that NC Cu-Ta retains a significant fraction of the thermal conductivity of pure coarse-grained Cu. Further, from advanced applications point of view, the advantage of NC Cu-Ta is that its room temperature thermal conductivity is at least 20–25 times that of Ni- or iron based alloys [6].To put this in perspective, the strength of the NC Cu-Ta alloy at 800 °C is about ~5 times higher than that of the best Nickel-based heat exchanger currently in used, along with a high thermal conductivity [6]. In addition, NC Cu-Ta exhibits the yield strength of over 1 GPa along with an 71% IACS electrical conductivity. It should be mentioned that the goal of designing materials with a high mechanical strength and minimal degradation of electric conductivity has been the subject of active research over the recent years. A comprehensive overview focusing on UFG and NC Cu and Al alloys has been recently published by Murashkin et al. [5]. It has been shown that bulk Cu alloys produced by severe plastic deformation can achieve a strength of hundreds of MPa while retaining much of the electric conductivity of CG Cu. The present work demonstrates that the NC Cu-Ta alloys exceed the existing envelope of the strength-conductivity combination by achieving the strength above 1 GPa with only moderate degradation of conductivity. Importantly, this favorable combination of mechanical and functional properties persists to unprecedentedly high temperatures due to the outstanding structural stability of the NC Cu-Ta alloys. Interestingly, the structure of these alloys is similar to the so-called "ideal" structure discussed in [5,14]. This structure was suggested to be the best for achieving the most favorable combination of strength (due to precipitation hardening), electric conductivity and thermal stability.

Overall, these findings demonstrate that the microstructural stability of NC Cu-Ta can lead to drastic increase in mechanical strength combined with favorable electric/thermal conductivities needed for various advanced applications.

Conclusions

We have addressed the fundamental question of whether fully stabilized NC materials have to exhibit the extreme SRS $(1 \geq m > 0.3)$ along with high electrical conductivity. The general view, until this point, has been that NC materials always exhibit this behavior starting at low homologous temperatures. Contrary to this expectation, the experimental evidence reported here reveals that NC Cu-Ta alloys (grain size <100 nm) do not exhibit a high SRS even at large homologous temperatures, nor do they show strain hardening, grain growth or texture formation. In support of this finding, atomistic computer simulations have shown that Ta nanoclusters slow down and eventually block grain boundary motion and grain rotation that are present in pure NC Cu. The suppression of these processes strongly reduces grain boundary sliding even at high temperatures without sacrificing plasticity. Taken together, the experiments and simulations provide convincing evidence that, contrary to the conventional belief, a truly stabilized NC material does not exhibit the highly elevated SRS behavior even when subjected to temperatures as high as 80% of the melting point. In fact, the NC Cu-Ta exhibits the lowest reported SRS at 80% of the melting point when compared to almost every structural material (Fig. 2b). Further, the suppression of the grain boundary processes through complex grain boundary-nanocluster interactions leads to the emergence of unique mechanical properties of NC materials; see property maps in Figs. 3 and 7. This discovery highlights a materials design principle through which materials with extraordinary strength (approximately one-half the theoretical limit), high electrical and thermal conductivity, and high-temperature stability can be developed for advanced technological applications. This work opens a new frontier towards developing structural and functional materials for extreme applications with properties that have been difficult to achieve via conventional approaches.

Methods

Powder processing and equal channel angular extrusion (ECAE)

Nanocrystalline (NC) Cu-10 at.%Ta powders were processed utilizing high-energy cryogenic mechanical alloying. Elemental Cu and Ta powders (−325 mesh and 99.9% purity) were loaded into a hardened steel vial in the appropriate proportion along with the milling media (440C stainless steel balls) inside a glove box with an Ar atmosphere (oxygen and H_2O are <1 ppm). The vials were loaded with 10 g of the Cu-Ta powder as well as the appropriate amount of media to ensure a ball-to-powder ratio of 5-to-1 by weight. A SPEX 8000 M shaker mill was utilized to perform the milling at cryogenic temperature (verified to be ~−196 °C) for 4 h using liquid nitrogen. The NC Cu-10 at.%Ta powder was consolidated to bulk via equal channel angular extrusion (ECAE). Before starting the ECAE process, the die assembly used for processing the billets was preheated to 623 K (350 °C) to minimize thermal loss during the ECAE processing. The billets, heated and equilibrated to 973 K (700 °C) for 40 min, were dropped into the ECAE tooling as quickly as possible from the furnace and extruded at an extrusion rate of 25.5 mm/s. These steps were repeated 4 times following route B_c [34–36] to prevent imparting a texture to the consolidated powder. By extruding through an angle of 90°, a total strain of 460% was imparted onto the powder-containing billet as a result of this processing. Specimens for mechanical testing were then machined from these billets, within the region containing the consolidated powder, via wire electric discharge machining into 3 mm length by 3 mm diameter cylinders. Further details related to the processing and impurity levels can be found in [19–21,37,38]. Also, the copper-tantalum system is an immiscible system, see the phase diagram below (Fig. A2a). Hence, we know that adding 10 atomic % of Ta would not change the melting temperature of the matrix (in this case, Cu) significantly. In fact, the basic differential thermal analyses plot shown below (Fig. A2-b-c) confirms that the melting temperature of Cu-10 at. % Ta is approximately the same as that of pure Cu.

Microstructural characterization

To obtain grain size distributions and microstructural characteristics, Transmission Electron Microscopy (TEM) was employed. TEM characterizations were carried out on the as-received and post-deformed conditions using an aberration corrected ARM-200F at 200 KeV. Multiple bright field and dark field images were captured in both the TEM and STEM modes to assess the microstructure and quantify statistics such as grain size distribution etc. For TEM characterizations, samples were prepared through conventional thinning procedures where a 3 mm disk from the bulk specimen was thinned to about 70 μm following which the specimens were dimpled to about a 5 μm thickness. Ion milling was performed using a Gatan Precision Ion Polishing System (PIPS) under liquid nitrogen temperatures to obtain electron-transparent regions in the specimens. The samples were also plasma cleaned in Ar prior to TEM observations to reduce contamination.

Mechanical characterization at quasi-static conditions

Quasi-static compression tests of specimens over a temperature range from ambient up to 1073 K (800 °C) were performed using an Instron load frame equipped with a 50 kN load cell and an ATS clam-shell heating furnace capable of a maximum temperature of 1473 K (1200 °C). The specimens for compression were cylinders 3 mm in diameter and length (aspect ratio 1.0). Compression tests were conducted at 298, 473, 573, 873, and 1073 K, with strain rates ranging from 8×10^{-4} to 1 s^{-1}. The system was held at the testing temperature for 30 min prior to loading to achieve a uniform temperature within the specimen. The push rods of the load frame were constructed of Inconel 718. Polished WC-disks lubricated with graphite were used as platens for compression testing. A thermocouple embedded in the Inconel rod was used to measure the temperature of the specimen. The stress–strain responses are shown in Fig. 2a. The compressive curves display an elastic- nearly perfectly plastic behavior over the entire temperature range with no significant strain hardening beyond 2.5% strain. Scanning electron images confirmed that a negligible oxide film (<10 μm in thickness) was formed on the surface of the cylinders as a result of exposure to the elevated temperatures, as measured post testing.

Post deformed microstructure analysis

The plastic deformation of the NC Cu-10 at.%Ta samples tested here was determined to occur either through deformation twinning or dislocation slip. Studies have indicated that grain boundaries serve as both nucleation sites and obstacles stopping the dislocations and causing their annihilation, absorption or transmission after they traverse the grain under an applied stress. The grain boundaries are thus responsible for obstructing the dislocation motion and controlling where the cross-slip between neighboring grains can occur [39–42].

To investigate the active deformation mechanisms and the reasoning behind the high-temperature and strain-rate response in these alloys, ex-situ microstructural characterization was performed using the same techniques as those employed to investigate the as-received microstructure. In general, the emissions of partial and full dislocations are competing mechanisms and their activation depends on the stress level and testing temperature. From the TEM observations on the NC-Cu-10 at.%Ta alloy presented here, an appreciable dislocation density was identified for the quasi-static testing conditions, implying the absence of dislocation absorption. In the case of conventional nanocrystalline materials, grain boundaries act as a source for dislocation generation. The dislocations are then free to traverse the grains and be absorbed at the opposite grain boundary acting as a sink. In the NC Cu-10 at.%Ta alloy, the dislocations are emitted, interact with the high density of nanoclusters, and become pinned at various sites, thereby reducing their mean free path of propagation [43].

Atomistic computer simulations

The atomistic simulations utilized the angular-dependent interatomic potential for the Cu-Ta system [44] reproducing a large number of physical properties of this system in agreement with experimental data and first-principles calculations. The MD simulations employed the Large-scale Atomic/Molecular Massively

Parallel Simulator (LAMMPS) [45]. The Monte Carlo (MC) simulations were conducted using the parallel MC code ParaGrandMC [46].

Two types of simulation samples were created: a bicrystal and a nanocrystal. The bicrystal represented a slab containing an isolated cylindrical grain embedded in a matrix grain. The slab had approximate dimensions 32 nm × 32 nm × 7.3 nm (6×10^5 - atoms) with periodic boundary conditions in all directions. It was initially filled with a perfect FCC Cu lattice whose <0 0 1> directions were parallel to the edges of the slab. A new grain was created by rotating a cylindrical region with a radius of 10 nm by an angle $\theta = 28.07°$ around the [0 0 1] direction parallel to the smaller dimension of the slab. A uniformly disordered Cu-Ta mixture was created by randomly substituting Cu atoms by Ta to match the target chemical composition. This random alloy served as the initial state for the subsequent MD simulations of the bicrystal evolution. The simulations utilized the NPT ensemble at the temperature of 900 K. Several chemical compositions were tested ranging from pure Cu to Cu-4 at.%Ta.

The Cu nanocrystal was constructed by the Voronoi tessellation method and contained 32 grains with an average grain size of 12.5 nm. The sample contained about 5.4 million atoms and had the approximate dimensions 40 nm × 40 nm × 40 nm with periodic boundary conditions in all directions. An equilibrium distribution of Ta was achieved by MC simulations at the temperatures of 300 and 800 K with the target composition of 4 at.%Ta. At these temperatures, no appreciable grain growth was observed during the MC simulations. The zero-pressure boundary conditions ensured that the introduction of the oversized Ta atoms did not create internal stresses. The samples were pre-strained by 2% to generate defects in the grain boundary structures. After thermal equilibration at a chosen temperature, each sample was subject to a 15% uniaxial compression with a constant strain rate while keeping zero stresses in the directions perpendicular to the compression. The compressive stress was monitored during the simulations and multiple snapshots were saved to follow the microstructure evolution.

Acknowledgements

M.R., S.T., C.K., and K.N.S. acknowledge the use of facilities within the LeRoy Eyring Center for Solid State Science at Arizona State University. This work was supported by Army Research Laboratory award number W911NF-15-2-0038 and the National Science Foundation award number 1663287. R.K.K and Y.M. were supported by the U.S. Army Research Office under contract number W911NF-15-1-007. K.A.D acknowledges A.J Roberts, M. Gallagher, and T. Luckenbaugh for synthesis of the Cu-Ta powder.

Competing interests

The authors declare no competing financial interests.

Data and materials availability

The data that support the findings are available from the corresponding authors upon request.

Appendix

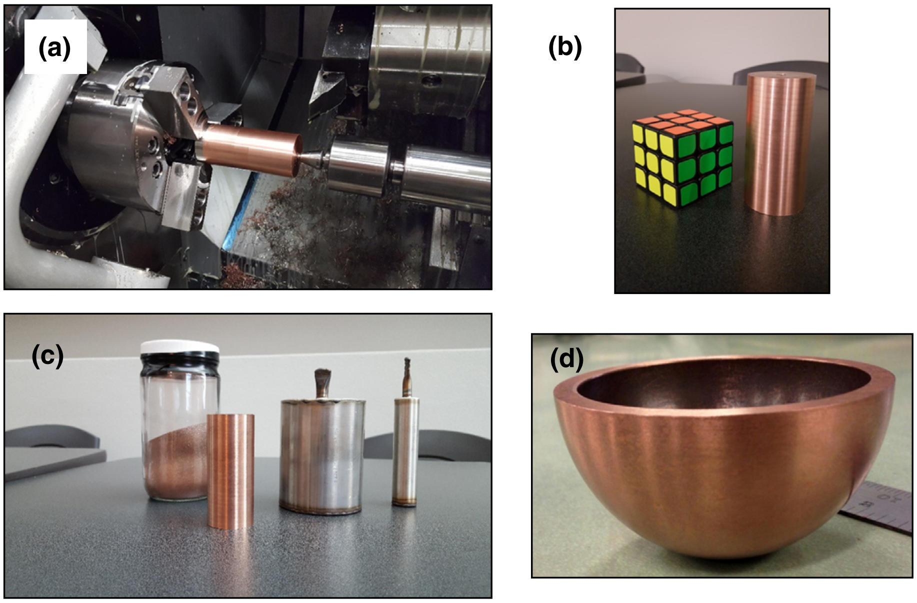

FIGURE A1

Complex geometry and shapes made of a NC Cu-Ta alloy. (a) 1.5 kg billet of fully consolidated nanocrystalline Cu-Ta alloy being turned down during a machining process [47]. (b) A close-up of large Cu-Ta rod. (c) 3 kg of Cu-Ta powder produced via high energy Zoz milling along with different sized and loaded hot isostatic press (HIP) cans and resultant billet of NC Cu-Ta. (d) 4 inch diameter near net shaped hemi-sphere produced by HIPing NC Cu-Ta powders to full density.

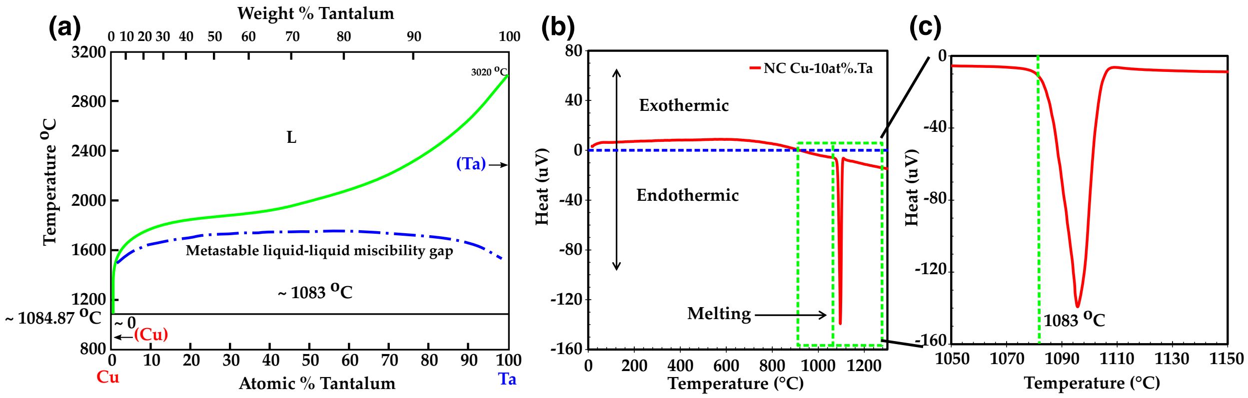

FIGURE A2

Determination of the melting point for NC Cu-Ta alloy. (a) Phase diagram for Cu and Ta. (b) DTA plot for NC Cu-Ta. (c) Zoomed view of DTA plot in (c) showing the onset of melting around 1083 °C. The melting temperature of pure Cu is 1085 °C.

References

[1] D.S. Gianola et al., Acta Mater. 54 (2006) 2253–2263.
[2] J.A. Sharon et al., Scr. Mater. 64 (2011) 25–28.
[3] I. Adlakha, K.N. Solanki, Sci. Rep. 5 (2015).
[4] T.J. Rupert, C.A. Schuh, Acta Mater. 58 (2010) 4137–4148.
[5] M.Y. Murashkin et al., J. Mater. Sci. 51 (2016) 33–49.
[6] X. Zhang et al., Heat Mas. Trans. 11 (2018), https://doi.org/10.5098/hmt.11.18.
[7] K. Spencer et al., Adv. Eng. Mater. 6 (2004) 290–297.
[8] J.T. Wood, J.D. Embury, M.F. Ashby, Acta Mater. 45 (1997) 1099–1104.
[9] L. Deng et al., J. Alloys Compd. 602 (2014) 331–338.
[10] Y. Sakai et al., IEEE Trans Magn. 28 (1992) 888–891.
[11] Y. Sakai et al., Appl. Phys. Lett. 59 (1991) 2965–2967.
[12] N.I. Kozlenkova et al., IEEE Trans. Magn. 32 (1996) 2921–2924.
[13] K. Han et al., Mater. Sci. Eng. A 267 (1999) 99–114.
[14] R.K. Islamgaliev et al., J. Appl. Phys. 115 (2014) 194301.
[15] V. Yamakov et al., Nat. Mater. 3 (2004) 43–47.
[16] J. Chen, L. Lu, K. Lu, Scr. Mater. 54 (2006) 1913–1918.
[17] Q. Wei et al., Mater. Sci. Eng. A 381 (2004) 71–79.
[18] K.A. Darling et al., Acta Mater. 76 (2014) 168–185.
[19] K.A. Darling et al., Nature 537 (2016) 378–381.
[20] M. Bhatia et al., Mater. Res. Lett. 5 (2017) 48–54.
[21] B.C. Hornbuckle et al., JOM 67 (2015) 2802–2809.
[22] W. Bochniak, Acta Metall. Mater. 43 (1995) 225–233.
[23] M. Zehetbauer, V. Seumer, Acta Metall. Mater. 41 (1993) 577–588.
[24] R.P. Carreker, W.R. Hibbard, Acta Metall. 1 (1953) 654–663.
[25] W.F. Gale, T.C. Totemeier, eds., in: Smithells Met. Ref. Book Eighth Ed., Butterworth-Heinemann, Oxford, 2004, p. iii..
[26] R.K. Koju et al., Acta Mater. 148 (2018) 311–319.
[27] Z. Trautt, Y. Mishin, Acta Mater. 60 (2012) 2407–2424.
[28] S. Srinivasan, J. Cahn, Sci. Technol. Interfaces (2002) 1–14.
[29] Y. Mishin, M. Asta, J. Li, Acta Mater. 58 (2010) 1117–1151.
[30] J.W. Cahn, Y. Mishin, A. Suzuki, Acta Mater. 54 (2006) 4953–4975.
[31] H.-A Kuhn, I. Altenberger, A. Käufler, H. Hölzl, M. Fünfer, in: L. Collini (Ed.), Copp. Alloys – Early Appl. Curr. Perform. – Enhancing Process, InTech Publisher, Rijeka, Croatia, 2012, pp. 51–68..
[32] C.R. Tellier, C.R. Pichard, A.J. Tosser, J. Phys. F Met. Phys. 9 (1979) 2377–2380.
[33] A.F. Mayadas, M. Shatzkes, Phys. Rev. B 1 (1970) 1382–1389.
[34] V.M. Segal, Mater. Sci. Eng. A 197 (1995) 157–164.
[35] M. Furukawa et al., J. Mater. Sci. 36 (2001) 2835–2843.
[36] Y.T. Zhu, T.C. Lowe, Mater. Sci. Eng. A 291 (2000) 46–53.
[37] M. Rajagopalan et al., Mater. Des. 113 (2017) 178–185.
[38] B.C. Hornbuckle et al., Scr. Mater. 160 (2019) 33–38.
[39] J. Schiøtz, K.W. Jacobsen, Science 301 (2003) 1357–1359.
[40] H. Van Swygenhoven, A. Caro, D. Farkas, Mater. Sci. Eng. A 309–310 (2001) 440–444.
[41] H.V. Swygenhoven, A. Caro, Appl. Phys. Lett. 71 (1997) 1652–1654.
[42] H. Van Swygenhoven, P.M. Derlet, A. Hasnaoui, Phys. Rev. B 66 (2002) 024101.
[43] C. Kale et al., Mater. Des. 163 (2019) 107551.
[44] G.P. Pun et al., Acta Mater. 100 (2015) 377–391.
[45] S. Plimpton, J. Comput. Phys. 117 (1995) 1–19.
[46] V.I. Yamakov, Parallel grand canonical Monte Carlo (ParaGrandMC) simulation code. Technical report number: NASA/CR-2016-219202, NF1676L-24373 (2016).
[47] V.H. Hammond, T.L. Luckenbaugh, M. Aniska, D.M. Gray, J.A. Smeltzer, B.C. Hornbuckle, C.J. Marvel, K.N. Solanki, T. Schmitz, K.A. Darling, Adv. Eng. Mater. 20 (2018) 1800405.